Juniper Online
Journal Material Science
ISSN: 2575-856X

Research Article
Volume 7 Issue 1 - April 2022
DOI: 10.19080/JOJMS.2022.07.555704

JOJ Material Sci

Hydrothermal Synthesis of Co_3O_4 Urchin-Like and their Catalytic Properties in Co Oxidation

Sami Barkaoui[1] and Gunel Imanova[2]*

[1]*Laboratory Materials Treatment and Analysis, National Institute for Research and Physico-chemical Analysis (INRAP), Tunisia*

[2]*Institute of Radiation Problems, Azerbaijan National Academy of Sciences, Azerbaijan*

Submitted: April 07, 2022; **Published:** April 19, 2022

***Corresponding author:** Gunel Imanova, Institute of Radiation Problems, Azerbaijan National Academy of Sciences, Azerbaijan

Abstract

Urchin-like nanocrystalline Co_3O_4 has been success fully prepared through a hydrothermal synthesis route via a simple and elegant route at low temperature, and was characterized by thermal analysis (TGA), X-ray diffraction (XRD), scanning electron microscopy (SEM), Raman spectroscopy, nitrogen adsorption/desorption isotherms and X-ray photoelectron spectroscopy (XPS). The light-off temperature (10% conversion) of CO oxidation on Co_3O_4 ursin-like catalyst was at 60°C and when the temperature reaches 120°C, the CO conversion ratio reaches 100%. The high relative concentration surface-adsorbed oxygen on the Co_3O_4 ursin-like is highly active in CO oxidation reaction due to its higher mobility than lattice oxygen. The study it has been shown that the high catalytic activity and stability for CO oxidation can be attributed to its higher mobility than lattice oxygen. In addition, the oxide defects can adsorb and activate gaseous O2 to form active oxygen species, which is beneficial to promote the CO oxidation reaction. The as-obtained results make the Co_3O_4 nanomaterial possible candidate to be used as catalyst for CO oxidation.

Keywords: Hydrothermal Synthesis; Urchin-Like; Nanocrystalline Co_3O_4; Catalytic Properties; Oxidation

Abbreviations: TGA: Thermal Analysis; XRD: X-ray Diffraction; SEM: Scanning Electron Microscopy; XPS: X-ray Photoelectron Spectroscopy; CO: Carbone monoxide; TCD: Thermal Conductivity Detector; BET: Brunauer-Emmett-Teller

Introduction

Carbone monoxide (CO), emission from mobile and stationary combustion sources is harmful to the environment, one of the major air pollutants and its presence even in traces may cause serious environmental and health problems. Therefore, the elimination of CO became important, and the oxidation of CO is a promising route to cleaning the air and lowering automotive emissions. Tricobalttetraoxide (Co_3O_4), a typical spinel-structure transition metal oxide, shows a strong morphology-dependence in the chemical reactions such as CO oxidation [1-6], CH4combustion [7], and selective reduction of NO with NH_3 [8]. For example, in 2009, it has been developed Co_3O_4 nanorods containing substantial amounts of exposed (110) planes exhibited superior catalytic activity for low-temperature CO oxidation to the spherical particles mainly enclosed by the (111) facets [1]. Also, Co_3O_4 nanotubes [9], nanosheets [3], nanowires [4], and nanocubes [10] similarly showed a distinct shape effect in CO oxidation. These results clearly confirm that controlling the morphology of nanostructured cobalt oxides is beneficial to expose more catalytically active sites.

Development of catalysts with desirable dimensions andmorphology is an interesting and challenging task owing to their improved catalytic activity and increasing applications in various fields [11-13]. Hierarchical 3D urchin-like nanostructures are promising for wastewater treatment through heterogeneous photo-catalysis because of their high surface area which facilitates catalysis by providing a larger solid-liquid interface. As can be seen from the writing information, radiation-heterogeneous forms in contact of to begin with radiation-oxidative treated zirconium and nano-zirconium oxide with water causes a alter within the sum of surface oxide film. The arrangement of an oxide film, in turn, changes the radiation-catalytic movement and physicochemical properties, which influence the dynamic parameters. One of them, the foremost delicate is the electro physical and optical properties of metal surfaces [14-22].

In this study, we report on the hydrothermal synthesis and physicochemical characterization of urchin-like nanostructures of Co_3O_4 with a surface area of 43m^2/g and their application in the CO reaction. The nanomaterial was synthesized using PEG-400 as a template. The Co_3O_4 morphology proved to be stable and did not collapse after calcination at 300°C for 2h. XRD measurements showed that the Co_3O_4 average particle size is 44nm. The as-synthesized C Co_3O_4 ursin-like exhibited superior catalytic activity and durability in CO oxidation at room temperature. It has been shown that when the temperature reaches to 120°C, the CO conversion ratio reaches 100%.

Experimental Details

Hydrothermal synthesis

The Co_3O_4 were synthesized by the typical procedures reported in the literature [23]. 0.77 mmol of $CoCl_2.6H_2O$ was dissolved in distilled water (27mL), followed by the addition of 0.25 mmol of PEG-400 then 8 mL of H_2O_2 (30%). The solution was transferred into a Teflon-lined stainless-steel autoclave which was sealed and maintained at 100°C for 12h. The autoclave was then cooled to 25°C, 2.25 mmol of urea was added and the autoclave was heated at 150°C for 16h. The precipitate was filtered, washed several times with deionized water and ethanol until free of chloride ions ($AgNO_3$ test) and dried overnight at 80°C under vacuum. Then, it was calcined in air at 300°C for 2h.

Characterization

TGA was performed using a Setaramsetsys 1750 apparatus at a heating rate of 2°C/min from RT to 700°C. XRD data were collected on a Panalytical X'Pert Pro diffractometer with CuK α radiation (λ = 1.5406 $\AA$) and a graphite monochromator by applying a step scanning method (2θ range from 10 to 70°). Raman spectroscopy was performed using a Jobin-Yvon T64000 spectrometer with a laser wavelength of 785 nm and a laser power of 3m W and taken after 60 seconds of exposure. The morphology of the sample was studied using an FEI Quanta 200 Environmental SEM and H_2-TPR profiles were obtained on a Micromeritics Autochem analyzer, in a Pyrex U-tube reactor and an on-line thermal conductivity detector (TCD). The calcined sample (50 mg) was first purged with an argon flow of 20 mL/min at a ramp rate of 10 °C/min to 350°C for 30 min to remove the traces of water, followed by cooling to room temperature. Then the sample was reduced by 4% vol. hydrogen and argon mixture (30 mL/min) at a temperature ramp rate of 5°C/min. The effluent gas was passed through a cooling trap to condense and collect the water produced during the reductions. The Brunauer-Emmett-Teller (BET) specific surface area, average pore diameter and pore size distributions were determined by N_2-physisorption at 77K using a Micrometrics ASAP-2020 instrument.

Catalytic investigation

CO oxidation was tested in a flow reactor. Before the reactions, Co_3O_4 was activated at 300°C for 1h at 5%O_2/He. After the sample was cooled down to room temperature, a feed gas (1%CO/20%O_2/He) was passed over the catalyst with a flow rate of 30 mL/min. 50 mg of the catalyst was heated to the desired reaction temperature and then kept for 1 hour until the catalyst reaction reached a steady state. The amounts of CO, CO_2 and O_2 in the inlet and outlet streams were analyzed by an online gas chromatograph. CO conversion was calculated from the measured CO concentration using the formula CO conversion = $[(Co_{in} - CO_{out})/CO_{in}]$, where CO_{in} and CO_{out} were the inlet and outlet CO concentration, respectively.

Result and Discussion

Thermo gravimetric analysis (TGA)

The thermal behavior of the hydrothermally as-prepared sample was examined using TGA in order to determine the appropriate calcination temperature. As depicted in Figure 1, a sharp decrease with a total weight loss of 11.2% around 260°C which indicated that a temperature of 300°C was chosen to completely decompose of cobalt chloride carbonate hydroxide hydrate decomposed completely into Co_3O_4, CO_2, Cl_2 and H_2O.

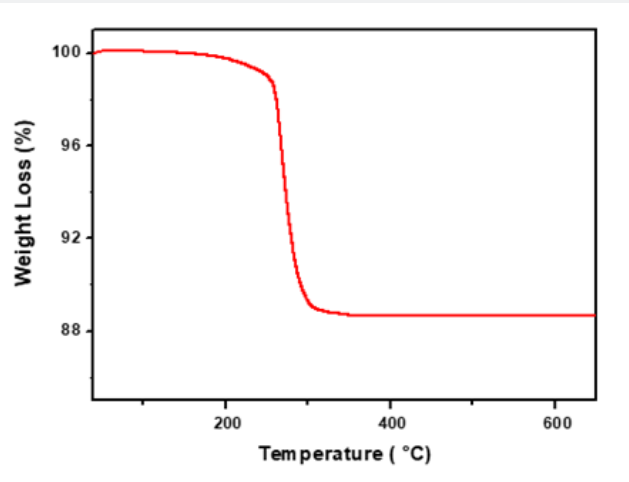

Figure 1: TGA curve in the air for as-prepared Co $(CO_3)_{0.35}Cl_{0.20}(OH)_{1.10}.1.74H_2O$ showing the transformation into Co_3O_4.

How to cite this article: Sami B, Gunel I. Enhanced Antiangiogenic Activity of Silver Nano-Particles Grafted on Graphene Oxide. JOJ Material Sci. 2022; 7(1): 555704. DOI: 10.19080/JOJMS.2022.07.555704

X-ray diffraction (XRD)

The diffraction patterns (XRD) are given in Figure 2. All the diffraction peaks displayed in the diffractogram (a) can be perfectly indexed to the cobalt chloride carbonate hydroxide hydrate [JCPDS 00-038-0547, Co $(CO_3)_{0.35}Cl_{0.20}(OH)_{1.10}.1.74H_2O$] and those in (b) with cobalt oxide [JCPDS 01-076-1802, Co_3O_4]. The second XRD pattern shows that the main peaks of the final products could be indexed to a cubic phase cobalt oxide and no peaks of other phases are observed. All the peaks can be indexed to the diffraction from the (111), (220), (311), (222), (400), (422), (511) and (440) planes of cubic Co_3O_4, respectively. Crystallite sizes (DXRD) for Co_3O_4 after heating in air at 300°C was estimated from the broadening of the most intense XRD peak (311) using the Debye-Scherrer approximation [24]. The average particle size of Co_3O_4 catalyst was calculated to be 44nm.

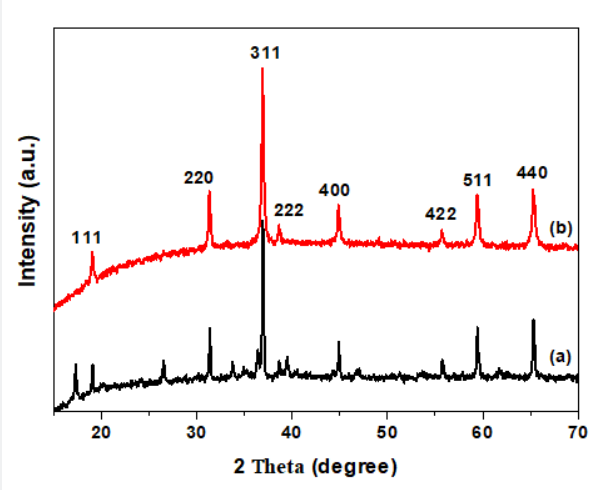

Figure 2: X-ray powder diffraction patterns of (b) the as-prepared catalyst before and (a) after calcination at 300°C for 2h.

Raman spectroscopy

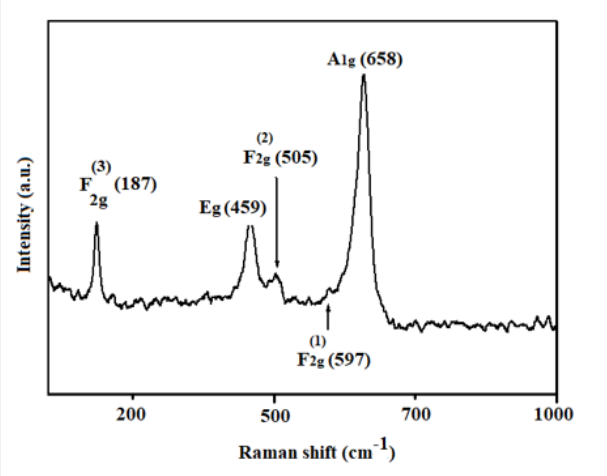

Figure 3: Raman spectrum of Co_3O_4 nanostructure calcined at 300°C in 100-1000 cm^{-1} range.

Raman spectroscopy of Co_3O_4 nanostructure is displayed in Figure 3. The Raman spectrum of the Co_3O_4 in the range of 100-800 cm^{-1} shows five obvious peaks (A_{1g} + E_g + $3F_{2g}$) located at around 187, 495, 505, 597 and 658 cm^{-1}, corresponding to the five Raman-active modes of Co_3O_4. The peak at 187 cm^{-1} is attributed to the $F^{(3)}2g$ mode of tetrahedral sites (CoO_4). The peaks at 459 and 505 cm_{-1} are assigned to the E_g and $F^{(2)}$ 2g symmetry, respectively. Whereas the peak at 597cm^{-1} is attributed to the $F^{(1)}_{2g}$ symmetry. The strong band at 658 cm^{-1} with A_{1g} symmetry is attributed to the characteristics of octahedral CoO6 sites corresponding to the

How to cite this article: Sami B, Gunel I. Enhanced Antiangiogenic Activity of Silver Nano-Particles Grafted on Graphene Oxide. JOJ Material Sci. 2022; 7(1): 555704. DOI: 10.19080/JOJMS.2022.07.555704

unique characteristics of spinel-type cubic Co_3O_4 phase [25,26] and no additional peaks assigned to other impurities such as Co_2O_3 and CoO have been found in good agreement with the XRD result. The Raman shifts are consistent with those of pure crystalline Co_3O_4, indicating that the Co_3O_4 catalyst has a similar crystal structure of the bulk Co_3O_4.

Scanning electronic microscopy (SEM)

Figures 4a & 4b shows the SEM images of the as-prepared precursor obtained by hydrothermal treatment at 150°C and after calcination at 300°C. As shown in Figure 4b, The Co_3O_4 morphology proved to be stable and did not collapse after calcination at 300°C in air for 2h. Polyethylene glycol (PEG) was used as a surfactant, which can modify the surface energy of the crystallographic surface. Co_3O_4 has a uniform urchin-like structure covered with dense nanowires starting from the center with an average of diameter of 4-6μm. The nanowires appear to have a common center and grow to the outside along the radial direction.

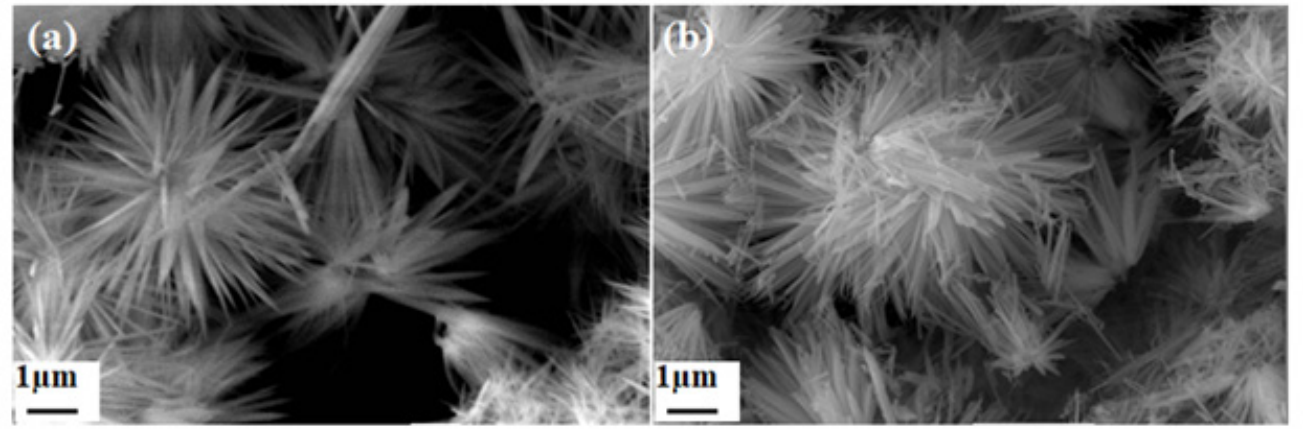

Figure 4: SEM images of (a) cobalt chloride carbonate hydroxide hydrate (b) the hierarchical uniform like of Co_3O_4 calcined at 300°C.

H_2-TPR studies

To further investigate the reducibility of the Co_3O_4 nanostructures, TPR measurements were carried out and shown in Figure 5. The H_2-TPR profile of the catalyst shows two main reduction peaks at about 360°C and 440°C, which can be attributed to the reduction of Co_3O_4 into CoO and from CoO to metallic Co [27], respectively. The narrow peaks indicate the reduction process was fast. The curve exhibits Co^{3+} is reduced at first, and then the produced Co^{2+} and Co^{2+} in the catalyst itself are further reduced into metallic Co.

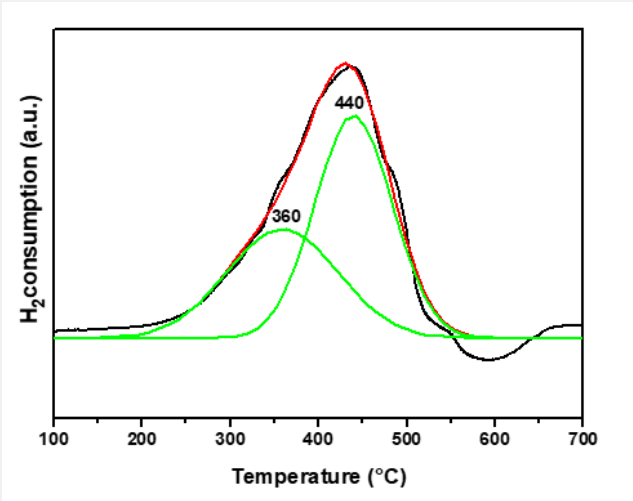

Figure 5: H_2-TPR profile of as-prepared Co_3O_4 ursin-like calcined at 300°C.

How to cite this article: Sami B, Gunel I. Enhanced Antiangiogenic Activity of Silver Nano-Particles Grafted on Graphene Oxide. JOJ Material Sci. 2022; 7(1): 555704. DOI: 10.19080/JOJMS.2022.07.555704

Nitrogen adsorption-desorption

As shown in Figure 6, The N_2 adsorption-desorption isotherms at 77 K which is close to type IV of the IUPAC classification [28] with an evident hysteresis loop in the 0.5 to 1.0 range suggesting that the Co_3O_4 ursin-like is basically mesoporous.

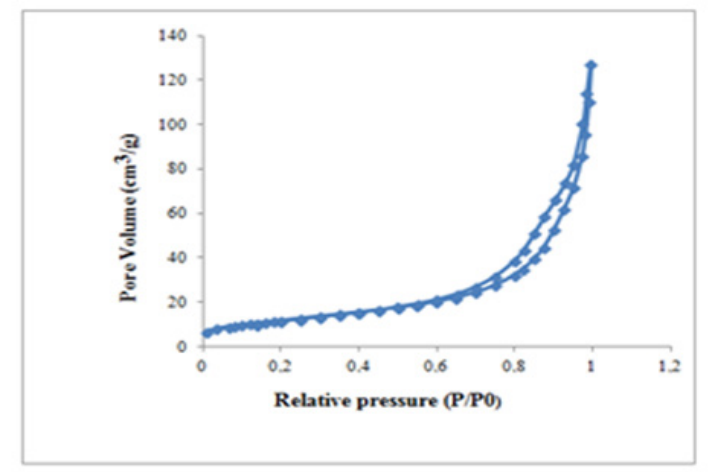

Figure 6: N_2-adsorption/desorption isotherms curve of Co_3O_4 calcined at 300°C.

The specific area of the sample calculated by BET to be 43m^2/g and the average pore diameters is 16 nm. These porous structures can be helpful for CO molecules to rapidly penetrate into the pores and contact to active sites during the catalytic process [29,30].

X-ray photoelectron spectroscopy (XPS)

XPS analysis was employed to investigate the surface elemental composition and chemical state of the as-obtained Co_3O_4-ursin like a catalyst, as shown in Figure 7. The XPS survey spectrum (Figure 7a) reveals that the sample only consists of cobalt and oxygen (the C1s peak was appeared, which could be due to the support used to prepare a sample for XPS analysis).The Co2p spectra in Figure 7b exhibited two major peaks with binding energies at around 780.0 eV and 795.1 eV corresponding to the Co2p3/2 and Co2p1/2, respectively, suggesting that the cobalt oxide was present in the form of Co_3O_4 [31,32].

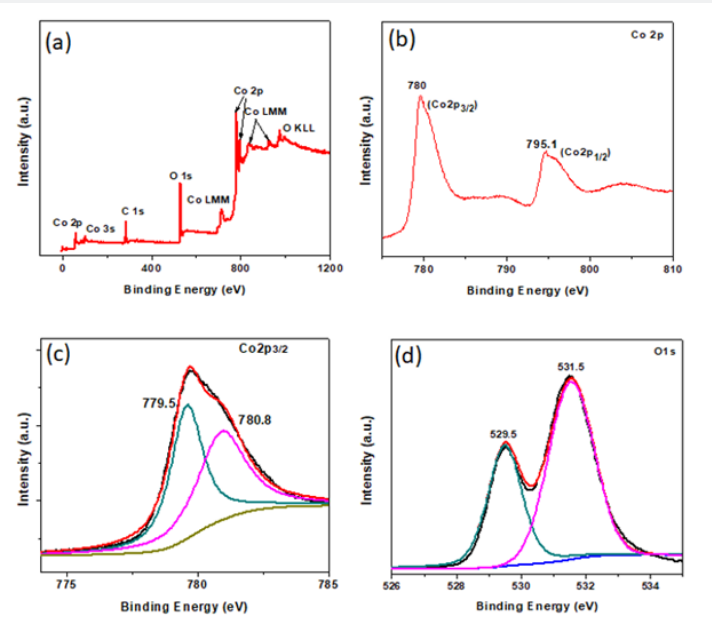

Figure 7: The XPS of as-obtained Co_3O_4 catalyst:(a) survey spectrum, (b) the Co2p XPS spectra of as-prepared catalyst, (c) the Co2p3/2 XPS spectra of as-prepared catalyst and (d) the O1s XPS spectra of the as-prepared catalyst.

How to cite this article: Sami B, Gunel I. Enhanced Antiangiogenic Activity of Silver Nano-Particles Grafted on Graphene Oxide. JOJ Material Sci. 2022; 7(1): 555704. DOI: 10.19080/JOJMS.2022.07.555704

Next, Co2p3/2 peaks in Figures 7b & 7c were fitted and de convoluted into two peaks of 780.8 and 779.5 eV, which are attributed to Co^{2+} and Co^{3+} respectively. As shown in Figure 7d, the O 1s electronic levels also were examined. The asymmetric O 1s could be de convoluted to two components at 531.5 and 529.5 eV. The XPS peak at 529.5 eV was attributed to the surface lattice oxygen (O_{latt}) species, and the 531.5 eV peak was ascribed to the surface adsorbed oxygen (O_{ads}) species in Co_3O_4 [33,34]. The O1s peak at 531.5 eV in the spectrum indicates the presence of surface adsorbed oxygen such as O_2^{2-} or O^-, belonging to defect-oxide or hydroxyl-like group [35,36]. The presence of surface hydroxyl like groups can result from oxygen vacancy on the surface of the Co_3O_4 catalyst originating from the dissociative adsorption of H_2O molecules. The oxide defects can adsorb and activate gaseous O_2 to form active oxygen species, which is beneficial to promote the oxidation reaction. Furthermore, Co_3O_4 ursin-like had the O_{ads}/O_{latt} ratio about 1.7 proving that its surface possesses the largest amount of facile and reactive oxygen species, which is beneficial to promote the CO oxidation reaction [37].

Catalytic properties of Co_3O_4 ursin-like in CO oxidation

As a typical probe reaction of numerous novel catalytic materials, CO oxidation was carried out to evaluate the catalytic activity of the as-prepared Co_3O_4 ursin-like. As shown in Figure 8a, the light-off temperature (10% conversion rate) at 60°C and when the temperature reaches to 120°C, the CO conversion ratio reaches 100%, which exhibits higher catalytic activity than that of the Co_3O_4 nanowires [4] and Co_3O_4 nanorods [38]. The long-term stability of the catalyst is important in practical applications. Furthermore, the stability test for CO oxidation was performed over the period of 20 h at T=120°C, as shown in Figure 8b. The high catalytic activity and stability for CO oxidation can be attributed to its higher mobility than lattice oxygen. In addition, the oxide defects can adsorb and activate gaseous O_2 to form active oxygen species, which is beneficial to promote the CO oxidation reaction.

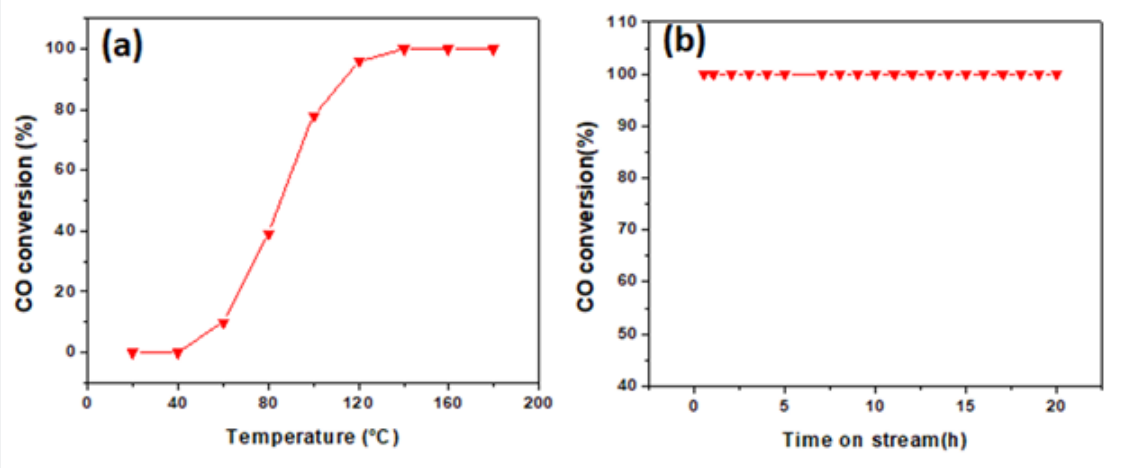

Figure 8: (a) Catalytic activity of Co_3O_4 oxide-ursin-like in the CO oxidation as the function of temperature, (b) durability tests of the Co_3O_4 ursin-like. Reaction conditions: the gas flow was composed of 1%CO/20%O_2/He (vol.) with a flow rate of 30 mL·min^{-1} and 50 mg catalysts were used.

Scanning electronic microscopy of the spent catalyst

As shown in Figure 9, the morphology of the spent catalyst after 20 h on stream reaction still retains ursin-like shape.

It can be shown that excellent catalytic performance and long-term stability for CO oxidation make the Co_3O_4 nanomaterial possible candidate to be used as a catalyst for CO oxidation.

Conclusion

In this paper, we have obtained Co_3O_4 precursor by a low-temperature hydrothermal method. The product Co_3O_4 has a uniform urchin-like structure covered with dense nanowires starting from the center with an average of diameter of 4-6 μm by PEG-400 as a template. The light-off temperature (10% conversion) of CO oxidation on Co_3O_4 ursin-like catalyst was at 60°C and when the temperature reaches to 120°C, the CO conversion ratio reaches 100%. The stability test for CO oxidation was performed over the period of 20h at T = 120°C. It has been shown that the high catalytic activity and stability for CO oxidation can be attributed to its higher mobility than lattice oxygen. In addition, the oxide defects can adsorb and activate gaseous O_2 to form active oxygen species, which is beneficial to promote the CO oxidation reaction. The as-obtained results make the Co_3O_4 nanomaterial possible candidate to be used as catalyst for CO oxidation.

How to cite this article: Sami B, Gunel I. Enhanced Antiangiogenic Activity of Silver Nano-Particles Grafted on Graphene Oxide. JOJ Material Sci. 2022; 7(1): 555704. DOI: 10.19080/JOJMS.2022.07.555704

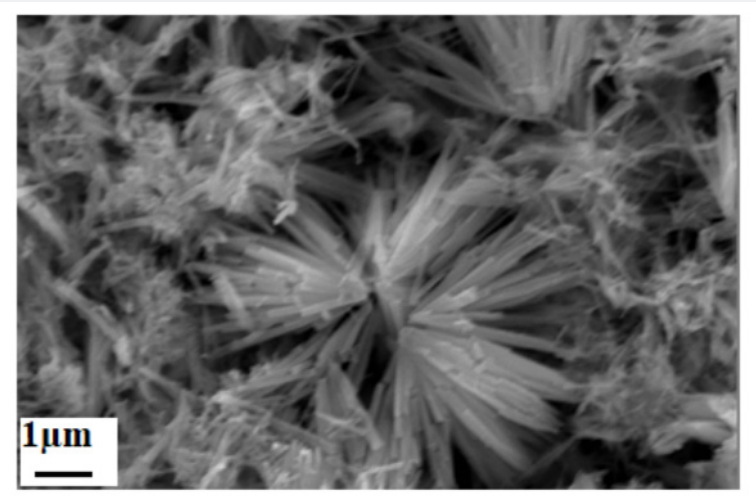

Figure 9: SEM image of the spent Co3O4 ursin-like after CO oxidation after 20 h on stream reaction at 120°C.

References

1. Xie X, Li Y, Liu ZQ, Haruta M, Shen W (2009) Low-temperature oxidation of CO catalysed by Co_3O_4 nanorods. Nature pp. 746-749.
2. Hu L, Sun K, Peng Q, Xu B, Li Y (2010) Surface active sites on Co_3O_4 nanobelt and nanocube model catalysts for CO oxidation. Nano Research 3: 363-368.
3. Xu C, Liu Y, Zhou C, Wang L, Geng H, et al. (2011) An *in Situ* Dealloying and Oxidation Route to Co_3O_4 Nanosheets and their Ambient-Temperature CO Oxidation Activity. Chem Cat Chem 3(2): 399-407.
4. Sun Y, Lv P, Yang JY, He L, Nie JC, et al. (2011) Ultrathin Co_3O_4 nanowires with high catalytic oxidation of CO. Chemical Communications 47: 11279-11281.
5. Teng Y, Kusano Y, Azuma M, Haruta M, Shimakawa Y (2011) Morphology effects of Co_3O_4 nanocrystals catalyzing CO oxidation in a dry reactant gas stream. Catalysis Science & Technology 1: 920-922.
6. Wang HF, Kavanagh R, Guo YL, Guo Y, Lu G, et al. (2012) Origin of extraordinarily high catalytic activity of Co_3O_4 and its morphological chemistry for CO oxidation at low temperature. Journal of catalysis 296: 110-119.
7. Hu L, Peng Q, Li Y (2008) Selective synthesis of Co_3O_4 nanocrystal with different shape and crystal plane effect on catalytic property for methane combustion. Journal of the American Chemical Society 130(48): 16136-16137.
8. Meng B, Zhao Z, Wang X, Liang J, Qiu J (2013) Selective catalytic reduction of nitrogen oxides by ammonia over Co_3O_4 nanocrystals with different shapes. Applied Catalysis B: Environmental 129: 491-500.
9. Lv Y, Li Y, Shen W (2013) Synthesis of Co_3O_4 nanotubes and their catalytic applications in CO oxidation. Catalysis Communications 42: 116-120.
10. Barkaoui S, Dhaouadi H, Kouass S, Touati F (2015) Structural and optical proprieties of doped cobalt oxide: $CuxCo_{3-x}O_4$ (x= 0.0; 0.1; 0.2; 0.4; and 0.6). Optik-International Journal for Light and Electron Optics 126(9-10): 1047-1051.
11. Ren Z, Guo Y, Liu CH, Gao PX (2013) Hierarchically nanostructured materials for sustainable environmental applications. Frontiers in chemistry 1: 18.
12. Sun P, Zhu Z, Zhao P, Liang X, Sun Y, et al. (2012) Gas sensing with hollow α-Fe_2O_3 urchin-like spheres prepared via template-free hydrothermal synthesis. Cryst Eng Comm 14: 8335-8337.
13. Lyons ME, Brandon MP (2010) A comparative study of the oxygen evolution reaction on oxidised nickel, cobalt and iron electrodes in base. Journal of Electroanalytical Chemistry 641(1-2): 119-130.
14. Imanova GT, Agayev TN, Jabarov SH (2021) Investigation of structural and optical properties of zirconia dioxide nanoparticles by radiation and thermal methods. Modern Physics Letters B 35(2).
15. Ali I, Imanova GT, Garibov AA, Agayev TN, Jabarov SH, et al. (2021) Gamma rays mediated water splitting on nano-ZrO_2 surface: Kinetics of molecular hydrogen formation. Radiation Physics and Chemistry 183: 109431.
16. Agayev TN, Musayeva ShZ, Imanova GT (2021) Studying the Kinetics of Formation of Molecular Hydrogen during the Radiolysis of Hexane and a Mixture of C_6H_{14}–H_2O on a Surface of n-ZrO_2. Russian Journal of Physical Chemistry A pp. 270–272.
17. Imran A, Gunel T, Imanova XY, Mbianda O, Alharbid ML (2022) Role of the radiations in water splitting for hydrogen generation. Sustainable Energy Technologies and Assessments 51: 1-44.
18. Imanova GT, Agaev TN, Garibov AA, Melikova SZ, Jabarov SH, et al. (2021) Radiation-thermocatalytic and thermocatalytic properties of n-ZrO_2-n-SiO_2 systems in the process of obtaining hydrogen from water at different temperatures. Journal of Molecular Structure1241: 130651.
19. Imanova GT (2020) Kinetics of Radiation-Heterogeneous and Catalytic Processes of Water in the Presence of Zirconia Nanoparticles. Advanced Physical Research pp. 94-101.
20. Imanova GT, Kaya M (2021) Importance of the Radiations in Radiolysis Processes for Hydrogen Generation. In: Book - Generis publishing. ISBN: 978-1-63902-693-7, pp. 50.
21. Imanova GT (2021) Gamma Rays Mediated Hydrogen Generation by Water Decomposition on Nano-ZrO_2 Surface. Modern Approaches on Material Science pp. 508-514.

How to cite this article: Sami B, Gunel I. Enhanced Antiangiogenic Activity of Silver Nano-Particles Grafted on Graphene Oxide. JOJ Material Sci. 2022; 7(1): 555704. DOI: 10.19080/JOJMS.2022.07.555704

22. Imanova G (2022) Molecular hydrogen production by radiolysis of water on the surface of nano-ZrO_2 under the influence of gamma rays. Synthesis and Sintering 2(1): 9-13.

23. Barkaoui S, Haddaoui M, Dhaouadi H, Raouafi N, Touati F (2015) Hydrothermal synthesis of urchin-like Co_3O_4 nanostructures and their electrochemical sensing performance of H_2O_2. Journal of Solid-State Chemistry 228: 226-231.

24. Huang R, Shen Y, Zhao L, Yan M (2012) Effect of hydrothermal temperature on structure and photochromic properties of WO_3 powder. Advanced Powder Technology 23(2): 211-214.

25. Zou G, Xu Y, Wang S, Chen M, Shangguan W (2015) The synergistic effect in Co-Ce oxides for catalytic oxidation of diesel soot. Catalysis Science & Technology 5: 1084-1092.

26. González PJ, López FR, Gutiérrez OJ, de Rivas B (2016) Oxidation of 1, 2-dichloroethane over nanocube-shaped Co_3O_4 catalysts. Applied Catalysis B: Environmental 199: 384-393.

27. Xie X, Shen W (2009) Morphology control of cobalt oxide nanocrystals for promoting their catalytic performance. Nanoscale 1: 50-60.

28. Armatas GS, Katsoulidis AP, Petrakis DE, Pomonis PJ, Kanatzidis MG (2010) Nanocasting of ordered mesoporous Co_3O_4-based polyoxometalate composite frameworks. Chemistry of Materials 22(20): 5739-5746.

29. Liuyun C, Kelin H, Qingruo X, Sze ML, Jin CS, et al. (2021) The enhancement of photocatalytic CO_2 reduction by the in situ growth of TiO_2 on Ti_3C_2 MXene. Catal Sci Technol 11: 1602-1614.

30. Mun LS, Sin JC, Lin H, Lim JW, Zeng H, et al. (2020) A Z-scheme WO_3 loaded-hexagonal rod-like ZnO/Zn photocatalytic fuel cell for chemical energy recuperation from food wastewater treatment. Appl Surf Sci 514: 145945.

31. Liu J, Zhao Z, Wang J, Xu C, Duan A, et al. (2008) The highly active catalysts of nanometric CeO_2-supported cobalt oxides for soot combustion. Applied Catalysis B: Environmental 84: 185-195.

32. Liu B, Liu Y, Hou H, Liu Y, Wang Q, et al. (2015) Variation of redox activity and synergistic effect for improving the preferential oxidation of CO in H_2-rich gases in porous Pt/CeO_2-Co_3O_4 catalysts. Catalysis Science & Technology 5: 5139-5152.

33. Xia Y, Dai H, Jiang H, Zhang L, Deng J, et al. (2011) Three-dimensionally ordered and wormhole-like mesoporous iron oxide catalysts highly active for the oxidation of acetone and methanol. Journal of hazardous materials 186: 84-91.

34. Xia Y, Dai H, Jiang H, Deng J, He H, et al. (2009) Mesoporous chromia with ordered three-dimensional structures for the complete oxidation of toluene and ethyl acetate. Environmental science & technology 43: 8355-8360.

35. Kang M, Park ED, Kim JM, Yie JE (2007) Manganese oxide catalysts for NO_x reduction with NH_3 at low temperatures. Applied catalysis A: general 327(2): 261-269.

36. Wu Z, Jin R, Liu Y, Wang H (2008) Ceria modified MnOx/TiO_2 as a superior catalyst for NO reduction with NH3 at low-temperature. Catalysis Communications 9(13): 2217-2220.

37. Liu F, He H, Ding Y, Zhang C (2009) Effect of manganese substitution on the structure and activity of iron titanate catalyst for the selective catalytic reduction of NO with NH_3. Applied Catalysis B: Environmental 93(1-2): 194-204.

38. Teng F, Chen M, Li G, Teng Y, Xu T, et al. (2011) High combustion activity of CH_4 and catalluminescence properties of CO oxidation over porous Co_3O_4 nanorods. Applied Catalysis B: Environmental 110: 133-140.

DOI: 10.19080/JOJMS.2022.07.555704

How to cite this article: Sami B, Gunel I. Enhanced Antiangiogenic Activity of Silver Nano-Particles Grafted on Graphene Oxide. JOJ Material Sci. 2022; 7(1): 555704. DOI: 10.19080/JOJMS.2022.07.555704